

Meson spectral functions with chirally symmetric lattice fermions

UKQCD Collaboration

Gert Aarts and Justin Foley

*Department of Physics, Swansea University
Singleton Park, Swansea, SA2 8PP, United Kingdom
E-mail: g.aarts@swan.ac.uk, j.foley@swansea.ac.uk*

ABSTRACT: In order to enhance our understanding of spectral functions in lattice QCD obtained with the help of the Maximum Entropy Method, we study meson spectral functions for lattice fermions with chiral symmetry. In particular we analyse lattice artefacts for standard overlap, overlap hypercube and domain wall fermions in the free field limit. We also present first results for pseudoscalar spectral functions in dynamical QCD with $2 + 1$ flavours of domain wall fermions, using data generated by the UKQCD and RBC collaborations on QCDOC machines.

KEYWORDS: Lattice Gauge Field Theories, Lattice QCD.

JHEP02(2007)062

Contents

1. Introduction	1
2. Spectral functions	2
3. Overlap fermions	5
4. Domain wall fermions	10
5. Overlap hypercube fermions	12
6. QCD with dynamical domain wall fermions	16
7. Summary	18
A. More on overlap hypercube fermions	19

1. Introduction

At zero temperature, the spectrum of QCD is encoded in hadronic spectral functions. Groundstates, excited states, decay widths and continuum contributions can, in principle, be extracted from spectral functions in different channels. Similarly, at finite temperature and/or density, medium modification of hadrons, the rate of photon and dilepton production, and hydrodynamical response functions can be obtained from the appropriate spectral functions.

Spectral functions are inherently real-time correlation functions and therefore difficult to obtain using standard lattice QCD data analysis techniques. Since euclidean lattice correlation functions are determined numerically on a finite number of points in imaginary time only, the analytical continuation to real time is classified as an ill-posed problem. In the past few years significant progress in the extraction of spectral functions from lattice QCD has come from the application of the Maximum Entropy Method (MEM) to this problem. MEM has been applied in many branches of science (see e.g. ref. [1] for a review), a thorough review focussing on lattice QCD can be found in ref. [2].

In order to interpret hadronic spectral functions obtained in lattice QCD, it is important to understand how lattice artefacts will appear. Lattice artefacts are expected to be present at large frequencies and may be studied in perturbation theory. Free lattice meson spectral functions have been studied at zero momentum for Wilson and hypercube fermions [3] and at nonzero momentum for Wilson and staggered fermions [4]. In this paper our first goal is to study lattice meson spectral functions for chirally symmetric fermions,

specifically overlap [5, 6], domain wall [7–9], and overlap hypercube [10, 11] fermions. Furthermore we present results for meson spectral functions obtained with the Maximum Entropy Method in QCD with 2+1 flavours of domain wall fermions, using data generated by the UKQCD and RBC collaborations on QCDOC machines.

The paper is organized as follows. In the next section we derive general expressions for free meson spectral functions on a finite lattice, independent of the particular fermion formulation that is used. In section 3 we specialize to overlap fermions and compare the resulting spectral functions, and in particular lattice artefacts, with continuum and staggered spectral functions. This analysis is extended to domain wall fermions in section 4 and to overlap hypercube fermions in section 5. In section 6 we present first results for pseudoscalar spectral functions in QCD with dynamical domain wall fermions. We find good agreement between the MEM results and the groundstate mass obtained with conventional cosh fits. We also argue that the structure seen at larger energies is consistent with lattice artefacts found in the first part of the paper, but a quantitative comparison requires further study.

2. Spectral functions

We start with a brief summary of well-known relations [2]. Euclidean meson correlators are defined by

$$G_H(\tau, \mathbf{x}) = \langle J_H(\tau, \mathbf{x}) J_H^\dagger(0, \mathbf{0}) \rangle, \tag{2.1}$$

where $J_H(\tau, \mathbf{x}) = \bar{\psi}(\tau, \mathbf{x}) \Gamma_H \psi(\tau, \mathbf{x})$ and $\Gamma_H = \{\mathbb{1}, \gamma_5, \gamma^\nu, \gamma^\nu \gamma_5\}$ for the scalar, pseudoscalar, vector and axial vector channels respectively. In general euclidean (and other) correlation functions are related to their spectral function via a dispersion relation in momentum space,

$$G_H(z, \mathbf{p}) = \int_0^\infty \frac{d\omega}{2\pi} \frac{\rho_H(\omega, \mathbf{p})}{\omega - z}, \tag{2.2}$$

where z is the frequency extended into the complex plane. Equating z to $i\omega_n$, where $\omega_n = 2\pi nT$ ($n \in \mathbb{Z}$) is the Matsubara frequency, yields the euclidean correlator at finite temperature T . In imaginary time this relation reads

$$G_H(\tau, \mathbf{p}) = \int_0^\infty \frac{d\omega}{2\pi} K(\tau, \omega) \rho_H(\omega, \mathbf{p}), \tag{2.3}$$

with the kernel

$$K(\tau, \omega) = \frac{\cosh[\omega(\tau - 1/2T)]}{\sinh(\omega/2T)}. \tag{2.4}$$

At zero temperature, this kernel reduces to $K(\tau, \omega) = e^{-\omega\tau}$.

In this section we derive a general expression for meson spectral functions on an isotropic lattice with $N_\sigma^3 \times N_\tau$ sites, by writing the euclidean correlators in the form (2.3) and identifying the lattice spectral function from that expression. We use periodic boundary conditions in space, $k_i = 2\pi n_i / N_\sigma$ with $n_i = -N_\sigma/2 + 1, -N_\sigma/2 + 2, \dots, N_\sigma/2 - 1, N_\sigma/2$ for $i = 1, 2, 3$, and antiperiodic boundary conditions in imaginary time, $k_4 = \pi(2n_4 + 1) / N_\tau$

with $n_4 = -N_\tau/2 + 1, -N_\tau/2 + 2, \dots, N_\tau/2 - 1, N_\tau/2$. Lattice units $a = 1$ are used throughout.

The correlators we are interested in are of the form

$$G_H(\tau, \mathbf{p}) = -\frac{N_c}{N_\sigma^3} \sum_{\mathbf{k}} \text{tr} S(\tau, \mathbf{k}) \Gamma_H S(-\tau, \mathbf{p} + \mathbf{k}) \Gamma_H, \quad (2.5)$$

where $S(\tau, \mathbf{k})$ is the fermion propagator and N_c denotes the number of colours. In order to derive compact expressions for lattice meson spectral functions, starting from eq. (2.5), we first discuss a generic fermion propagator, without specifying a particular formulation. We consider the following fermion propagator

$$S(K) = \frac{1}{D(K)} \left[-i \sum_{\nu=1}^4 C_\nu(K) \gamma_\nu \sin k_\nu + m(K) \right], \quad (2.6)$$

where K denotes the four-momentum. The functions $C_\nu(K)$, $m(K)$ and $D(K)$ depend on the fermion formulation, but they are all invariant under $k_\nu \rightarrow -k_\nu$. In order to be able to use eq. (2.5), we construct the fermion propagator in the mixed representation,

$$S(\tau, \mathbf{k}) = \frac{1}{N_\tau} \sum_{k_4} e^{ik_4\tau} S(K). \quad (2.7)$$

We assume that $S(K)$ has a single pole at $k_4 = \pm iE_{\mathbf{k}}$, determined by $D(iE_{\mathbf{k}}, \mathbf{k}) = 0$. In the case of more than one pole, a summation over the poles is required. This yields [14]

$$S(\tau, \mathbf{k}) = \gamma_4 S_4(\tau, \mathbf{k}) + \sum_{i=1}^3 \gamma_i S_i(\tau, \mathbf{k}) + \mathbb{1} S_u(\tau, \mathbf{k}), \quad (2.8)$$

where

$$\begin{aligned} S_4(\tau, \mathbf{k}) &= S_4(\mathbf{k}) \cosh(\tilde{\tau} E_{\mathbf{k}}), \\ S_i(\tau, \mathbf{k}) &= S_i(\mathbf{k}) \sinh(\tilde{\tau} E_{\mathbf{k}}), \\ S_u(\tau, \mathbf{k}) &= S_u(\mathbf{k}) \sinh(\tilde{\tau} E_{\mathbf{k}}). \end{aligned} \quad (2.9)$$

Here $0 \leq \tau < N_\tau = 1/T$ and $\tilde{\tau} = \tau - 1/2T$. The momentum-dependent coefficients read

$$\begin{aligned} S_4(\mathbf{k}) &= \frac{C_4(iE_{\mathbf{k}}, \mathbf{k})}{2\mathcal{E}_{\mathbf{k}}} \frac{\sinh E_{\mathbf{k}}}{\cosh(E_{\mathbf{k}}/2T)}, \\ S_i(\mathbf{k}) &= \frac{C_i(iE_{\mathbf{k}}, \mathbf{k})}{2\mathcal{E}_{\mathbf{k}}} \frac{i \sin k_i}{\cosh(E_{\mathbf{k}}/2T)}, \\ S_u(\mathbf{k}) &= -\frac{m(iE_{\mathbf{k}}, \mathbf{k})}{2\mathcal{E}_{\mathbf{k}} \cosh(E_{\mathbf{k}}/2T)}, \end{aligned} \quad (2.10)$$

where

$$\frac{1}{2\mathcal{E}_{\mathbf{k}}} = i \text{Res}_{k_4=iE_{\mathbf{k}}} \frac{1}{D(K)}. \quad (2.11)$$

The propagator satisfies $S(-\tau, \mathbf{k}) = \gamma_5 S^\dagger(\tau, \mathbf{k}) \gamma_5$.

	Γ_H	$a_H^{(1)}$	$a_H^{(2)}$	$a_H^{(3)}$		Γ_H	$a_H^{(1)}$	$a_H^{(2)}$	$a_H^{(3)}$
ρ_S	$\mathbb{1}$	1	-1	1	ρ_{PS}	γ_5	1	-1	-1
ρ^{00}	γ^0	1	1	1	ρ_5^{00}	$\gamma^0 \gamma_5$	1	1	-1
ρ^{ii}	γ^i	3	-1	-3	ρ_5^{ii}	$\gamma^i \gamma_5$	3	-1	3
ρ_V	γ^μ	2	-2	-4	ρ_A	$\gamma^\mu \gamma_5$	2	-2	4

Table 1: Coefficients $a_H^{(i)}$ for free spectral functions in different channels H . In the case of γ^i and $\gamma^i \gamma_5$, the sum is taken over $i = 1, 2, 3$; $\rho_V = \rho^{ii} - \rho^{00}$ and $\rho_A = \rho_5^{ii} - \rho_5^{00}$.

For reference, we note that for fermions in the continuum one finds the same propagator, with the replacements $\mathcal{E}_{\mathbf{k}} \rightarrow E_{\mathbf{k}}$, $\sinh E_{\mathbf{k}} \rightarrow E_{\mathbf{k}}$, $\sin k_i \rightarrow k_i$, $m(iE_{\mathbf{k}}, \mathbf{k}) \rightarrow m$ and $C_\nu \rightarrow 1$.

Inserting eq. (2.8) in eq. (2.5) gives the euclidean correlator

$$G_H(\tau, \mathbf{p}) = \frac{4N_c}{N_\sigma^3} \sum_{\mathbf{k}} \left[a_H^{(1)} S_4(\tau, \mathbf{k}) S_4^\dagger(\tau, \mathbf{r}) - a_H^{(2)} \sum_i S_i(\tau, \mathbf{k}) S_i^\dagger(\tau, \mathbf{r}) - a_H^{(3)} S_u(\tau, \mathbf{k}) S_u^\dagger(\tau, \mathbf{r}) \right], \quad (2.12)$$

where $\mathbf{r} = \mathbf{p} + \mathbf{k}$. The coefficients $a_H^{(i)}$ are given in table 1.¹

We will now extract the lattice meson spectral functions. It is straightforward to write the above expression for $G_H(\tau, \mathbf{p})$ as

$$G_H(\tau, \mathbf{p}) = \int_0^\infty \frac{d\omega}{2\pi} K(\tau, \omega) \rho_H^{\text{lattice}}(\omega, \mathbf{p}), \quad (2.13)$$

and identify the expressions for the lattice spectral functions [4]

$$\begin{aligned} \rho_H^{\text{lattice}}(\omega, \mathbf{p}) = \frac{4\pi N_c}{N_\sigma^3} \sum_{\mathbf{k}} \sinh\left(\frac{\omega}{2T}\right) \left\{ \right. \\ & \left[a_H^{(1)} S_4(\mathbf{k}) S_4^\dagger(\mathbf{r}) + a_H^{(2)} \sum_i S_i(\mathbf{k}) S_i^\dagger(\mathbf{r}) + a_H^{(3)} S_u(\mathbf{k}) S_u^\dagger(\mathbf{r}) \right] \delta(\omega + E_{\mathbf{k}} - E_{\mathbf{r}}) \\ & + \left[a_H^{(1)} S_4(\mathbf{k}) S_4^\dagger(\mathbf{r}) - a_H^{(2)} \sum_i S_i(\mathbf{k}) S_i^\dagger(\mathbf{r}) - a_H^{(3)} S_u(\mathbf{k}) S_u^\dagger(\mathbf{r}) \right] \delta(\omega - E_{\mathbf{k}} - E_{\mathbf{r}}) \\ & \left. + (\omega \rightarrow -\omega) \right\}. \end{aligned} \quad (2.14)$$

This expression is the immediate counterpart of the continuum result [4]

$$\begin{aligned} \rho_H^{\text{cont}}(\omega, \mathbf{p}) = 2\pi N_c \int \frac{d^3k}{(2\pi)^3} \frac{1}{E_{\mathbf{k}} E_{\mathbf{r}}} \left\{ \right. \\ & [n_F(E_{\mathbf{k}}) - n_F(E_{\mathbf{r}})] \left[a_H^{(1)} E_{\mathbf{k}} E_{\mathbf{r}} + a_H^{(2)} \mathbf{k} \cdot \mathbf{r} + a_H^{(3)} m^2 \right] \delta(\omega + E_{\mathbf{k}} - E_{\mathbf{r}}) \\ & + [1 - n_F(E_{\mathbf{k}}) - n_F(E_{\mathbf{r}})] \left[a_H^{(1)} E_{\mathbf{k}} E_{\mathbf{r}} - a_H^{(2)} \mathbf{k} \cdot \mathbf{r} - a_H^{(3)} m^2 \right] \delta(\omega - E_{\mathbf{k}} - E_{\mathbf{r}}) \\ & \left. - (\omega \rightarrow -\omega) \right\}, \end{aligned} \quad (2.15)$$

¹We use Minkowski gamma-matrices to label the channels, see ref. [4] for further details.

where $n_F(\omega) = 1/[\exp(\omega/T) + 1]$ is the Fermi distribution, as can be seen by making the appropriate substitutions. At zero temperature, only the “1” in the second term survives. In the continuum the remaining three-dimensional integral can be carried out for arbitrary external momentum and quark mass. Analytical expressions for continuum meson spectral functions can be found in ref. [4]. Since the expressions are lengthy, we give here the result at vanishing external momentum only,

$$\begin{aligned} \rho_H^{\text{cont}}(\omega, \mathbf{0}) = & \Theta(\omega^2 - 4m^2) \frac{N_c}{8\pi} \sqrt{1 - \frac{4m^2}{\omega^2}} \left[1 - 2n_F\left(\frac{\omega}{2}\right) \right] \\ & \left[\omega^2 \left(a_H^{(1)} - a_H^{(2)} \right) + 4m^2 \left(a_H^{(2)} - a_H^{(3)} \right) \right] \\ & - 4\pi\omega\delta(\omega)N_c \int \frac{d^3k}{(2\pi)^3} \frac{n'_F(\omega_{\mathbf{k}})}{\omega_{\mathbf{k}}^2} \left[k^2 \left(a_H^{(1)} + a_H^{(2)} \right) + m^2 \left(a_H^{(1)} + a_H^{(3)} \right) \right]. \end{aligned} \tag{2.16}$$

The first term contributes above threshold ($\omega > 2m$), while the contribution proportional to $\omega\delta(\omega)$ is related to conserved quantities (see e.g. ref. [15] in relation to transport coefficients). Note that spectral functions are odd, $\rho_H(-\omega, \mathbf{p}) = -\rho_H(\omega, \mathbf{p})$.

On the lattice the spectral functions (2.14) can in general not be evaluated analytically. Instead, in the following sections we give the explicit expressions for the free fermion dispersion relation $E_{\mathbf{k}}$, the coefficients $S_4(\mathbf{k})$, $S_i(\mathbf{k})$ and $S_u(\mathbf{k})$, and the residue $\mathcal{E}_{\mathbf{k}}$, for overlap, domain wall and overlap hypercube fermions. We use those in eq. (2.14) to compute lattice spectral functions by performing the spatial lattice sum over \mathbf{k} numerically, using the same approach as in refs. [3, 4].

3. Overlap fermions

The massless overlap (Neuberger) operator is given by

$$D_N = \mu \left(1 + \frac{X}{\sqrt{X^\dagger X}} \right), \quad X = D_W - \mu, \tag{3.1}$$

where D_W the usual Wilson-Dirac operator and μ is a constant.² In momentum space, X reads

$$X(K) = i \sum_{\nu} \gamma_{\nu} \sin k_{\nu} + b(K), \quad b(K) = r \sum_{\nu} (1 - \cos k_{\nu}) - \mu. \tag{3.2}$$

The corresponding fermion propagator is

$$S(K) = \frac{1}{2\mu} \left(\frac{-i \sum_{\nu} \gamma_{\nu} \sin k_{\nu}}{\omega(K) + b(K)} + 1 \right), \tag{3.3}$$

with

$$\omega(K) = \sqrt{X^\dagger X} = \sqrt{\sum_{\nu} \sin^2 k_{\nu} + b^2(K)}. \tag{3.4}$$

The poles of the propagator are determined by $\omega(K) + b(K) = 0$, which yields

$$\sum_{\nu} \sin^2 k_{\nu} = 0, \quad b(K) < 0. \tag{3.5}$$

²In other studies the coefficient μ is sometimes denoted by ρ .

Writing $k_4 = iE_{\mathbf{k}}$ gives the dispersion relation

$$\cosh E_{\mathbf{k}} = \sqrt{1 + \mathcal{K}_{\mathbf{k}}^2}, \quad b(iE_{\mathbf{k}}, \mathbf{k}) < 0, \quad (3.6)$$

where we defined

$$\mathcal{K}_{\mathbf{k}}^2 = \sum_i \sin^2 k_i. \quad (3.7)$$

The constraint $b < 0$ arises from the square root in the definition of $\omega(K)$.³ Due to this constraint, there is only a pole when \mathbf{k} is not too large, and there are no solutions near the edges of the Brillouin zone. Apart from this, the dispersion relation is identical to the one for naive fermions.

Meson spectral functions for free massless overlap fermions take the form (2.14) of the previous section, with the now explicitly determined functions (2.10)

$$C_\nu(iE_{\mathbf{k}}, \mathbf{k}) = 1, \quad S_u(\mathbf{k}) = 0, \quad (3.8)$$

and the residue (2.11)

$$\frac{1}{\mathcal{E}_{\mathbf{k}}} = \frac{\omega(iE_{\mathbf{k}}, \mathbf{k})}{\mu \sinh E_{\mathbf{k}} \cosh E_{\mathbf{k}}}. \quad (3.9)$$

Chiral symmetry is manifest in the meson spectral functions, since the expressions in the scalar (vector) and the pseudoscalar (axial vector) channel only differ with respect to the coefficient $a_H^{(3)}$, see table 1. Since $S_u = 0$, dependence on $a_H^{(3)}$ vanishes for massless overlap fermions.

The extension to massive overlap fermions is straightforward. To include the mass, the overlap operator is changed to

$$D_{\text{ov}, m_0} = \left(1 - \frac{m_0}{2\mu}\right) D_N + m_0, \quad (3.10)$$

and the corresponding propagator is

$$S(K) = \frac{1}{2} \frac{(\mu - m_0/2) [-i \sum_\nu \gamma_\nu \sin k_\nu + b(K)] + (\mu + m_0/2)\omega(K)}{(\mu^2 + m_0^2/4)\omega(K) + (\mu^2 - m_0^2/4)b(K)}. \quad (3.11)$$

We find that the pole is determined by

$$\sum_\nu \sin^2 k_\nu = -\bar{m}_0^2 b^2(K), \quad (\mu^2 - m_0^2/4) b(K) < 0, \quad (3.12)$$

where we defined

$$\bar{m}_0 = \frac{\mu m_0}{\mu^2 + m_0^2/4}. \quad (3.13)$$

We always consider m_0 to be small (in lattice units), while $\mu \sim 1$, so that the constraint still implies $b < 0$. Writing again $k_4 = iE_{\mathbf{k}}$ and solving the resulting quadratic equation gives the allowed dispersion relation

$$\cosh E_{\mathbf{k}} = \frac{1}{1 - r^2 \bar{m}_0^2} \left[-r \bar{m}_0^2 \mathcal{M}_{\mathbf{k}} + \sqrt{(1 + \mathcal{K}_{\mathbf{k}}^2)(1 - r^2 \bar{m}_0^2) + \bar{m}_0^2 \mathcal{M}_{\mathbf{k}}^2} \right], \quad (3.14)$$

³Provided that $0 < \mu < 2r$, there is no pole at $k_4 = \pi - iE_{\mathbf{k}}$, since then the constraint cannot be met.

provided that

$$b(iE_{\mathbf{k}}, \mathbf{k}) = -r \cosh E_{\mathbf{k}} + \mathcal{M}_{\mathbf{k}} < 0. \quad (3.15)$$

Here we have defined

$$\mathcal{M}_{\mathbf{k}} = r - \mu + r \sum_i (1 - \cos k_i). \quad (3.16)$$

At zero momentum, the rest mass is determined by

$$\cosh E_0 = \frac{1}{1 - r^2 \bar{m}_0^2} \left[r(\mu - r) \bar{m}_0^2 + \sqrt{1 + \bar{m}_0^2 \mu (\mu - 2r)} \right], \quad (3.17)$$

while at small \mathbf{k} and m_0 eq. (3.14) reduces to

$$\cosh E_{\mathbf{k}} = 1 + \frac{1}{2} (\mathbf{k}^2 + m_0^2) + \dots, \quad (3.18)$$

as expected.

We compare the massive overlap dispersion relation with the naive (or staggered) dispersion relation,

$$\cosh E_{\mathbf{k}} = \sqrt{1 + \mathcal{K}_{\mathbf{k}}^2 + m_0^2}, \quad (3.19)$$

and the continuum expression $E_{\mathbf{k}} = \sqrt{\mathbf{k}^2 + m_0^2}$ in figure 1 for two values of the overlap parameter μ and a rest mass $m_R \equiv E_0 = 0.1$ (the HF kernel shown as well will be discussed below). Throughout this paper we take $r = 1$. We find that the overlap dispersion relation can hardly be distinguished from the naive one for the value of m_R shown here. In the overlap case the dispersion relation terminates before the edge of the Brillouin zone due to the constraint $b < 0$. The momentum value of the endpoint depends on the overlap parameter μ and increases with increasing μ .

The coefficients in the meson spectral functions now read

$$C_\nu(iE_{\mathbf{k}}, \mathbf{k}) = 1 - \frac{m_0}{2\mu}, \quad m(iE_{\mathbf{k}}, \mathbf{k}) = \frac{m_0}{\mu + m_0/2} \omega(iE_{\mathbf{k}}, \mathbf{k}), \quad (3.20)$$

and the residue is

$$\frac{1}{\mathcal{E}_{\mathbf{k}}} = \frac{\mu}{\mu^2 + m_0^2/4} \frac{1}{\cosh E_{\mathbf{k}} + \bar{m}_0^2 r b(iE_{\mathbf{k}}, \mathbf{k})} \frac{\omega(iE_{\mathbf{k}}, \mathbf{k})}{\sinh E_{\mathbf{k}}}. \quad (3.21)$$

Comparison between these functions at small momentum and their continuum counterparts shows that there is a multiplicative renormalization of the fermion propagator at finite m_0 . This is not unexpected since the kinetic term in (3.11) has a nonstandard normalization. One way to write the renormalization factor is to compare the expressions at zero spatial momentum. Explicitly, the renormalization factor is given by

$$C_\nu(iE_0, \mathbf{0}) \frac{E_0}{\mathcal{E}_0}. \quad (3.22)$$

At small K and m_0 , the euclidean fermion propagator (3.11) is approximately given by

$$S(K) \approx \frac{\mu^3 (\mu - m_0/2)}{(\mu^2 + m_0^2/4)^2} \left[\frac{-iK + m_0}{K^2 + m_0^2} + \frac{1}{2\mu} \right]. \quad (3.23)$$

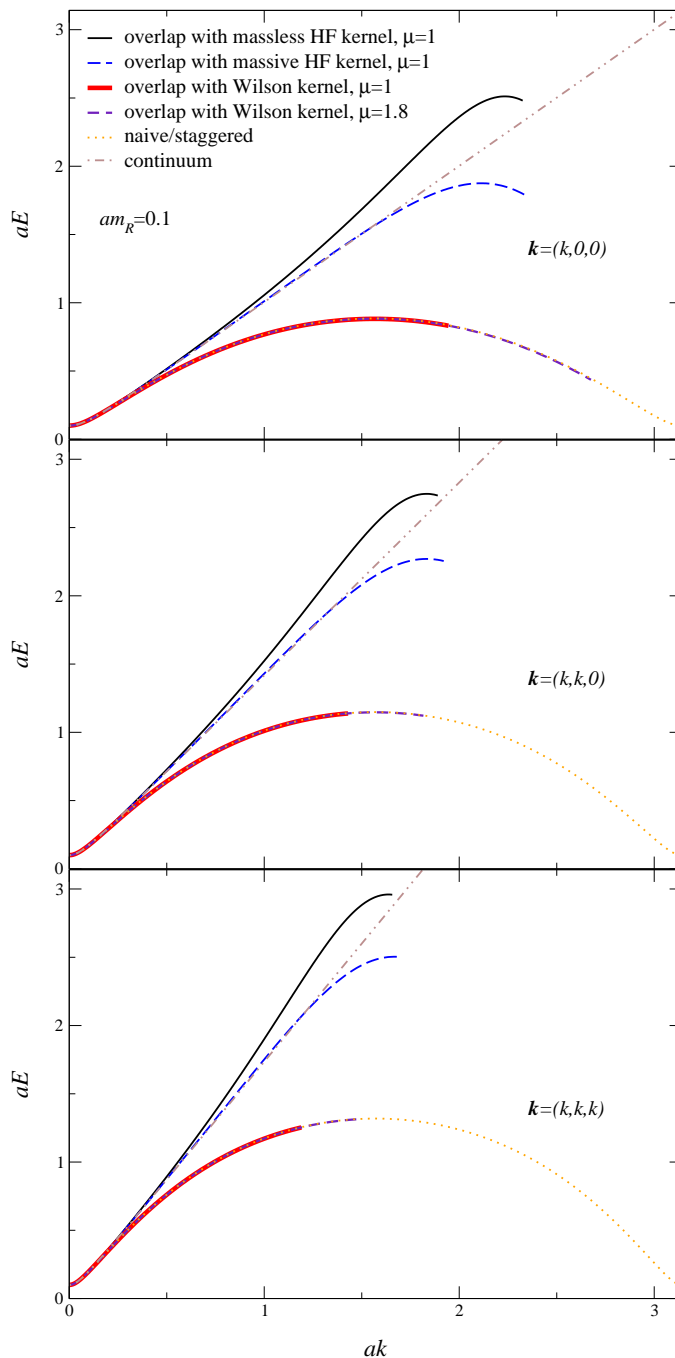


Figure 1: Dispersion relation along three directions in the Brillouin zone for massive overlap fermions with rest mass $m_R = 0.1$ using a massive/massless HF kernel with $\mu = 1$ and a standard Wilson kernel with $\mu = 1, 1.8$. For comparison the naive and continuum dispersion relation are shown as well.

The multiplicative prefactor goes to 1 in both the chiral and the continuum limit.

We now have all the ingredients to compute spectral functions with free overlap fermions. In figure 2 we show the pseudoscalar spectral function at zero momentum for

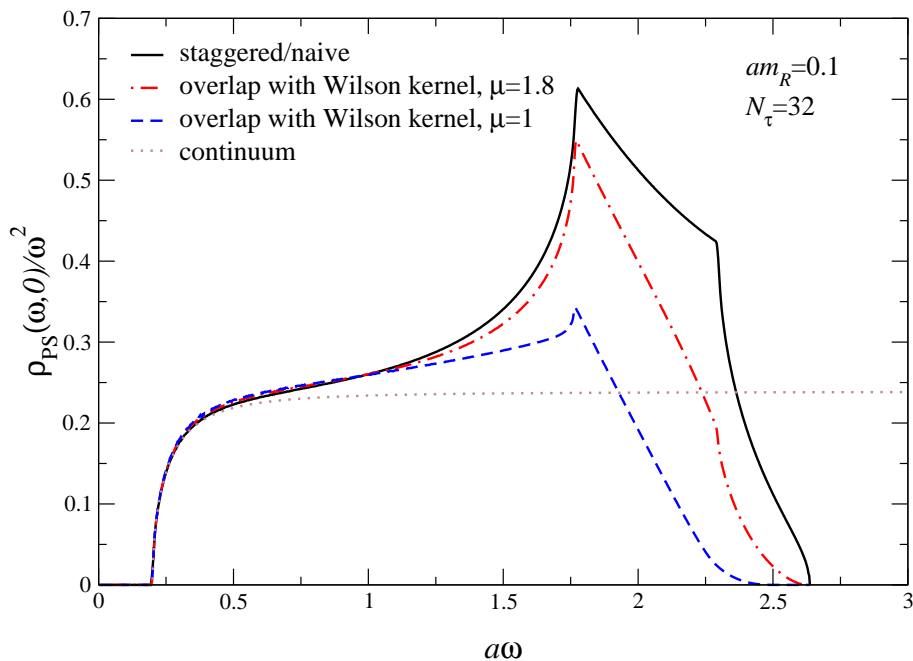


Figure 2: Pseudoscalar spectral functions $\rho_{\text{PS}}(\omega, \mathbf{0})/\omega^2$ for staggered and standard overlap fermions with $\mu = 1, 1.8$, and $m_R = 0.1, N_\tau = 32$.

overlap fermions with $\mu = 1$ and 1.8 , staggered fermions and the continuum result (2.17). All spectral functions increase in the same manner beyond the threshold $\omega = 2m_R$, provided that m_R is small. At larger frequencies, effects due to the deviation of the continuum and lattice dispersion relation become visible. The first cusp is due to the maximal lattice energy reached at $\mathbf{k} = (\pi/2, 0, 0)$ (cf. figure 1 top), which yields a cusp at $a\omega \approx 2 \cosh^{-1} \sqrt{2} \approx 1.76$. The difference in height of the spectral functions is due to the different residues, which depends on μ for overlap fermions and for staggered fermions is given by [4]

$$\frac{1}{\mathcal{E}_{\mathbf{k}}} = \frac{1}{\cosh E_{\mathbf{k}} \sinh E_{\mathbf{k}}}. \tag{3.24}$$

For staggered fermions, there is a second cusp due to the maximal lattice energy reached at $\mathbf{k} = (\pi/2, \pi/2, 0)$. For overlap fermions this cusp is absent (for $\mu = 1$) or less pronounced (for $\mu = 1.8$), since the constraint has terminated the dispersion relation (cf. figure 1 middle). The maximal energy is given by $\omega_{\text{max}} = 2E_{\mathbf{k}_{\text{max}}}$, which for staggered fermions is reached at $\mathbf{k} = (\pi/2, \pi/2, \pi/2)$ and given by $a\omega \approx 2 \cosh^{-1} 2 \approx 2.63$. For overlap fermions, this region is again modified due to the constraint.

The effect of finite N_τ is shown in figure 3 for overlap fermions with $\mu = 1$ and is seen to be negligible for large enough values of N_τ .

Finally, lattice spectral functions at nonzero momentum are similar to the continuum ones in the small frequency region $a\omega \lesssim 0.5$ and lattice artefacts at larger ω are not affected by the external momentum, provided that the external momentum is small (see ref. [4] for further details).

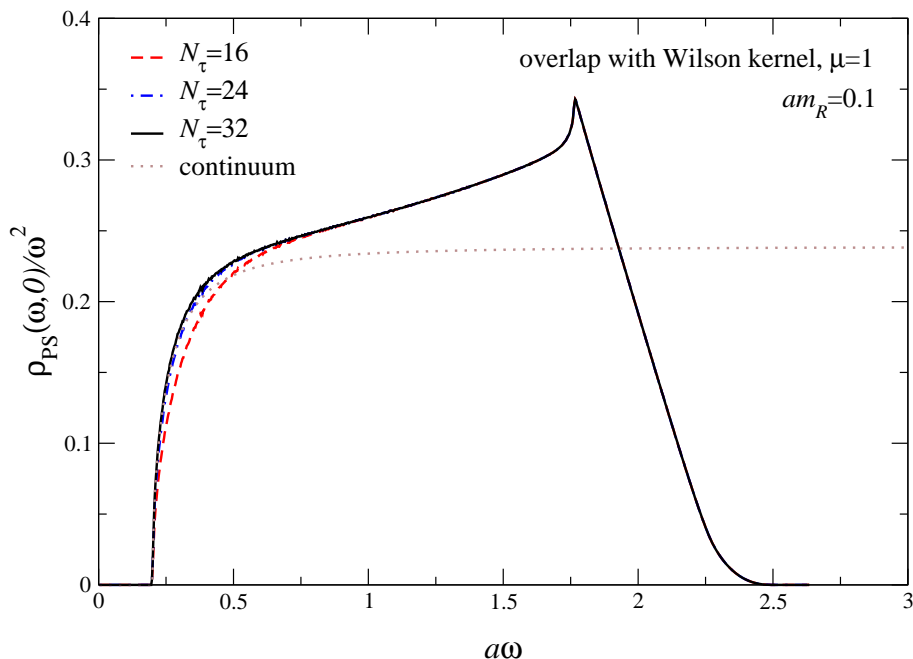


Figure 3: N_τ dependence of the pseudoscalar spectral function $\rho_{\text{PS}}(\omega, \mathbf{0})/\omega^2$ for standard overlap fermions ($\mu = 1, m_R = 0.1$).

4. Domain wall fermions

The four-dimensional massive domain wall propagator, assuming an infinite extent of the fifth dimension, reads

$$S(K) = \frac{-i \sum_\nu \gamma_\nu \sin k_\nu + m_0 (1 - |W|e^{-\alpha})}{e^\alpha |W| - 1 + m_0^2 (1 - |W|e^{-\alpha})}, \quad (4.1)$$

where

$$\cosh \alpha = \frac{1 + W^2 + \sum_\nu \sin^2 k_\nu}{2|W|}, \quad (4.2)$$

$$W = 1 - \mu + \sum_\nu (1 - \cos k_\nu). \quad (4.3)$$

The domain wall height is denoted with μ and is taken between 0 and 2. For small momentum and $1 < \mu < 2$, W is negative (see e.g. ref. [16] for a recent review).

The dispersion relation is determined by the pole in the propagator at $k_4 = iE_{\mathbf{k}}$. Again we find a quadratic equation for $\cosh E_{\mathbf{k}}$, with the allowed solution

$$\cosh E_{\mathbf{k}} = \frac{x_{\mathbf{k}} + (1 + m_0^2)\sqrt{y_{\mathbf{k}}}}{z_{\mathbf{k}}}, \quad (4.4)$$

with

$$\begin{aligned} x_{\mathbf{k}} &= -2m_0^2 (1 + \mathcal{M}_{\mathbf{k}}) [1 + \mathcal{K}_{\mathbf{k}}^2 + \mathcal{M}_{\mathbf{k}}(2 + \mathcal{M}_{\mathbf{k}})], \\ y_{\mathbf{k}} &= (1 + \mathcal{K}_{\mathbf{k}}^2) (1 - m_0^2)^2 + m_0^2 [1 + \mathcal{K}_{\mathbf{k}}^2 - \mathcal{M}_{\mathbf{k}}(2 + \mathcal{M}_{\mathbf{k}})]^2, \\ z_{\mathbf{k}} &= (1 - m_0^2)^2 - 4m_0^2 \mathcal{M}_{\mathbf{k}}(2 + \mathcal{M}_{\mathbf{k}}), \end{aligned} \quad (4.5)$$

where $\mathcal{M}_{\mathbf{k}}$ is given in eq. (3.16) with $r = 1$.

For massless domain wall fermions, eq. (4.4) reduces to

$$\cosh E_{\mathbf{k}} = \sqrt{1 + \mathcal{K}_{\mathbf{k}}^2}, \quad (4.6)$$

as in the overlap formalism. The rest mass is determined by

$$\cosh E_0 = \frac{2m_0^2(\mu - 2)^3 + (1 + m_0^2)\sqrt{1 + m_0^2(2 + \mu(\mu - 4)(\mu - 2)^2) + m_0^4}}{1 - 2m_0^2(2\mu^2 - 8\mu + 7) + m_0^4}. \quad (4.7)$$

Expanding the massive case for small \mathbf{k} and m_0 , we find

$$\cosh E_{\mathbf{k}} = 1 + \frac{1}{2}(\mathbf{k}^2 + m_{\text{eff}}^2) + \dots, \quad (4.8)$$

where $m_{\text{eff}} = (1 - w_0^2)m_0$ is the multiplicatively renormalized fermion mass. The multiplicative factor reads

$$1 - w_0^2 = \mu(2 - \mu), \quad w_0 = W(0) = 1 - \mu. \quad (4.9)$$

In the limit that $m_0 \ll 1$, $m_R = m_{\text{eff}}$. The constraint on the allowed fermion energies arises in this case from the behaviour of the propagator in the fifth direction: demanding a normalizable solution of the five-dimensional Dirac equation yields the constraint

$$|W(iE_{\mathbf{k}}, \mathbf{k})| < 1, \quad (4.10)$$

both in the massless and the massive case.⁴

The resulting dispersion relation (4.4) is indistinguishable from the dispersion relation for massive overlap fermions for small values of m_0 , shown in figure 1. At finite values of m_0 , deviations are more pronounced for larger values of μ .

The coefficients in the meson spectral functions read

$$C_\nu(iE_{\mathbf{k}}, \mathbf{k}) = 1, \quad m(iE_{\mathbf{k}}, \mathbf{k}) = m_0 \left(1 - \frac{1}{2}A_-\right), \quad (4.11)$$

and the residue reads

$$\frac{1}{\mathcal{E}_{\mathbf{k}}} = \frac{2}{A_+ (1 + \mathcal{M}_{\mathbf{k}}) - 2W + m_0^2 [A_- (1 + \mathcal{M}_{\mathbf{k}}) - 2W]} \frac{\sqrt{A^2 - 4W^2}}{\sinh E_{\mathbf{k}}}. \quad (4.12)$$

Here we defined

$$A_{\pm} = A \pm \sqrt{A^2 - 4W^2}, \quad A = 1 + W^2 - \sinh^2 E_{\mathbf{k}} + \mathcal{K}_{\mathbf{k}}^2, \quad (4.13)$$

and all quantities are evaluated onshell at $K = (iE_{\mathbf{k}}, \mathbf{k})$. In the massless case the residue simplifies considerably to

$$\frac{1}{\mathcal{E}_{\mathbf{k}}} = \frac{1 - W^2(iE_{\mathbf{k}}, \mathbf{k})}{\cosh E_{\mathbf{k}} \sinh E_{\mathbf{k}}}. \quad (4.14)$$

⁴We note here that $W(iE_{\mathbf{k}}, \mathbf{k})$ is always larger than -1 , so that this constraint coincides with $b(iE_{\mathbf{k}}, \mathbf{k}) < 0$ in the overlap formalism, since $W = 1 + b$.

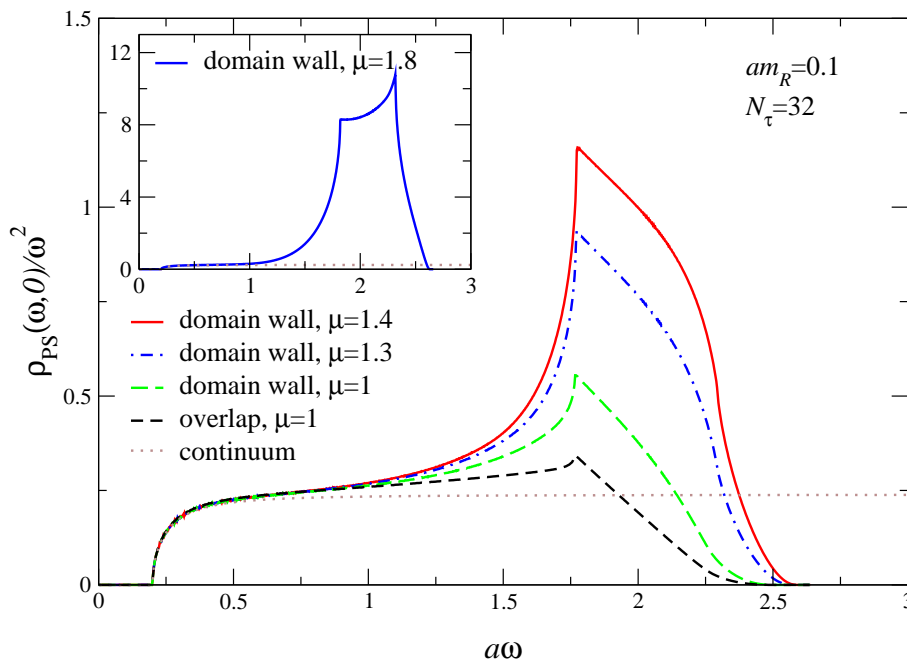


Figure 4: Pseudoscalar spectral functions $\rho_{PS}(\omega, \mathbf{0})/\omega^2$ for domain wall fermions (with $\mu = 1, 1.3, 1.4$ and $\mu = 1.8$ in the inset) and standard overlap fermions (with $\mu = 1$).

At small K and m_0 , the euclidean fermion propagator is approximately given by

$$S(K) \approx (1 - w_0^2) \frac{-iK + m_{\text{eff}}}{K^2 + m_{\text{eff}}^2}, \quad (4.15)$$

which suggests a multiplicative renormalization factor $1 - w_0^2$. However, we have found numerically that corrections to this renormalization factor are large for small but finite m_0 and larger values of μ . From a comparison of the expressions at zero spatial momentum, we find the multiplicative factor to be

$$\frac{E_0}{\mathcal{E}_0}, \quad (4.16)$$

which deviates substantially from $1 - w_0^2$ for the largest value of μ used here. The resulting spectral functions are shown in figure 4 for different values of μ . To obtain these spectral functions, we fix the rest mass $m_R = 0.1$ and solve for the bare mass m_0 using eq. (4.7). Subsequently we find the multiplicative factor using (4.16) to properly set the vertical scale.

As can be seen in figures 4 and 2, the spectral functions obtained from overlap and domain wall fermions differ at larger frequencies. The overlap spectral functions show reduced discretization effects. We note that is due to the difference in residues, and not because of the dispersion relations. Increasing the domain wall height shows that the μ dependence is much stronger than in the overlap case. For $\mu = 1.8$ the effect is remarkably large.

5. Overlap hypercube fermions

The overlap formalism solves the chirality problem in lattice QCD. However, its disper-

	massless HF	massive HF		massless HF	massive HF
$\rho^{(1)}$	0.136846794	0.054580	$\lambda^{(0)}$	1.852720547	1.268851
$\rho^{(2)}$	0.032077284	0.011010	$\lambda^{(1)}$	-0.060757866	-0.030083
$\rho^{(3)}$	0.011058131	0.003255	$\lambda^{(2)}$	-0.030036032	-0.010830
$\rho^{(4)}$	0.004748991	0.001206	$\lambda^{(3)}$	-0.015967620	-0.004716
			$\lambda^{(4)}$	-0.008426812	-0.002212

Table 2: Coefficients $\rho^{(a)}$ and $\lambda^{(a)}$ in the hypercube action for massless ($m_R = 0$) and massive ($m_R = 1$) hypercube fermions.

sion relation shows no reduction in discretisation effects when compared to e.g. staggered fermions. A systematic approach to constructing fermion actions which have good chiral properties and very small discretisation errors is based on the renormalisation group (RG). In this approach one aims to approximate so-called ‘perfect actions’, which lie on the renormalized trajectory of an RG transformation [17, 18]. Here we consider a particular truncation of a perfect action, the hypercube fermion (HF) action introduced in ref. [19]. This action is obtained from an RG transformation which yields an ultralocal action in one dimension [20]. For a recent review, see ref. [21].

The hypercube action is written as

$$S = \sum_{x,y} \bar{\psi}(x) \left\{ \sum_{\nu} \gamma_{\nu} \rho_{\nu}(x-y) + \lambda(x-y) \right\} \psi(y), \tag{5.1}$$

where the couplings ρ_{ν} and λ are nonzero only if x and y are in the same hypercube. Explicitly, the corresponding Dirac operator reads, in momentum space,

$$D_{\text{HF}}(K) = i \sum_{\nu} C_{\nu}^{\text{HF}}(K) \gamma_{\nu} \sin k_{\nu} + m_{\text{HF}}(K), \tag{5.2}$$

with

$$C_{\nu}^{\text{HF}}(K) = 2\rho^{(1)} + 4\rho^{(2)} \sum_{\sigma \neq \nu} \cos k_{\sigma} + 8\rho^{(3)} \sum_{\sigma \neq \nu} \prod_{\eta \neq \nu, \sigma} \cos k_{\eta} + 16\rho^{(4)} \prod_{\sigma \neq \nu} \cos k_{\sigma}, \tag{5.3}$$

and

$$m_{\text{HF}}(K) = \lambda^{(0)} + 2\lambda^{(1)} \sum_{\nu} \cos k_{\nu} + 4\lambda^{(2)} \sum_{\nu} \sum_{\sigma > \nu} \prod_{\eta \neq \nu, \sigma} \cos k_{\eta} + 8\lambda^{(3)} \sum_{\nu} \prod_{\sigma \neq \nu} \cos k_{\sigma} + 16\lambda^{(4)} \prod_{\nu} \cos k_{\nu}. \tag{5.4}$$

The coefficients $\rho^{(a)}$ and $\lambda^{(a)}$ are determined by requiring that this action reproduces the perfect action on a finite volume with sides of length 3, and periodic boundary conditions, see table 2 for two examples.

In the limit of zero momentum, the action coefficients satisfy

$$C_{\nu}^{\text{HF}}(0) = 2 \left[\rho^{(1)} + 6\rho^{(2)} + 12\rho^{(3)} + 8\rho^{(4)} \right] = \left(\frac{m_R}{e^{m_R} - 1} \right)^2, \tag{5.5}$$

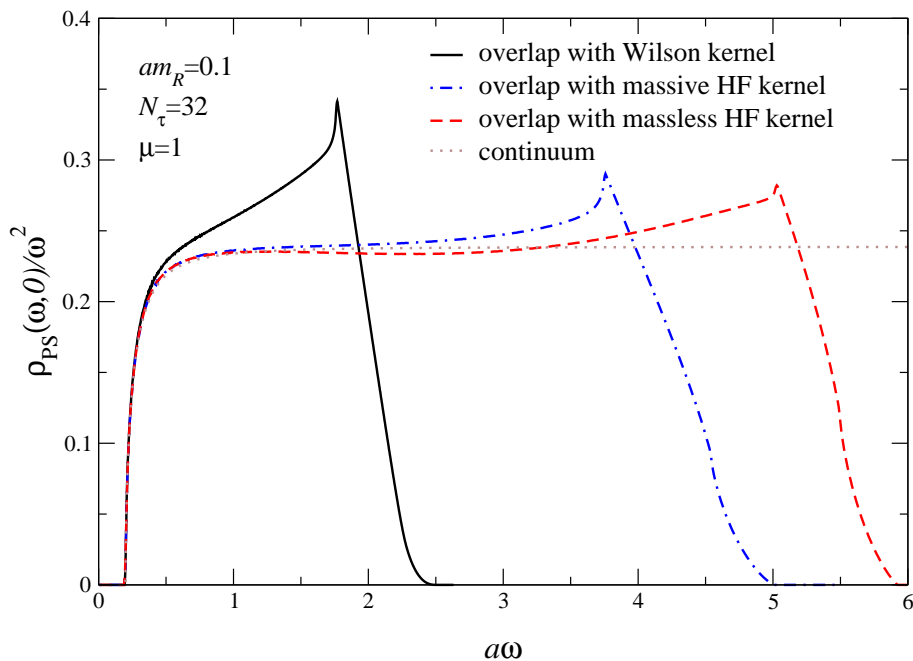


Figure 5: Pseudoscalar spectral functions $\rho_{\text{PS}}(\omega, \mathbf{0})/\omega^2$ for overlap fermions with a standard and a massless/massive HF kernel ($\mu = 1$, $m_R = 0.1$, $N_\tau = 32$).

$$m_{\text{HF}}(0) = \lambda^{(0)} + 8\lambda^{(1)} + 24\lambda^{(2)} + 32\lambda^{(3)} + 16\lambda^{(4)} = \frac{m_R^2}{e^{m_R} - 1}, \quad (5.6)$$

where $m_R = E_{\mathbf{0}}$ is the rest mass in HF dispersion relation. These relations follow from the expression for the one-dimensional fixed point action, which can be evaluated explicitly, and ultimately they depend on the RG transformation used to construct the action.

The truncation involved in the construction of the hypercube action introduces chiral symmetry breaking and discretisation errors. If the truncation is justified, these effects will be small.⁵ Following ref. [11], exact chiral symmetry can be restored by using the hypercube operator as the kernel for the overlap operator. The resulting overlap operator should inherit many of the properties of the kernel and, in particular, have much smaller cutoff effects than the standard overlap operator.

To determine the expression for the overlap hypercube propagator we first write the expression for the kernel, $X = D_{\text{HF}} - \mu$, in momentum space, and

$$X(K) = i \sum_{\nu} C_{\nu}^{\text{HF}}(K) \gamma_{\nu} \sin k_{\nu} + b(K), \quad b(K) = m_{\text{HF}}(K) - \mu. \quad (5.7)$$

The corresponding propagator for massive overlap fermions is obtained by multiplying $\sin k_{\nu}$ with $C_{\nu}^{\text{HF}}(K)$ in eq. (3.11) of section 3. Writing $k_4 = iE_{\mathbf{k}}$, the dispersion relation is again determined by a quadratic equation for $\cosh E_{\mathbf{k}}$. Since the explicit expressions are rather lengthy, we have listed them in appendix A.

⁵For studies of meson spectral functions using hypercube fermions in quenched QCD, see refs. [12, 13].

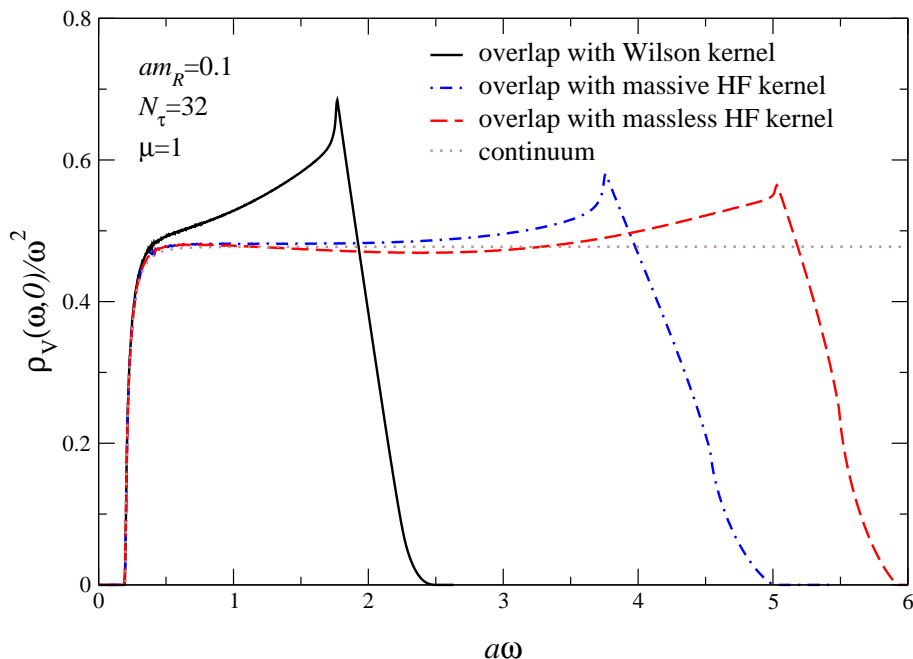


Figure 6: As in figure 5 for the vector spectral function $\rho_V(\omega, \mathbf{0})/\omega^2$.

In the limit of small \mathbf{k} and m_0 , we find that the overlap HF dispersion relation reduces to

$$\cosh E_{\mathbf{k}} = 1 + \frac{1}{2} (\mathbf{k}^2 + m_{\text{eff}}^2) + \dots \quad (5.8)$$

where the renormalized fermion mass is

$$m_{\text{eff}} = \frac{\mu - m_{\text{HF}}(0)}{\mu C_{\nu}^{\text{HF}}(0)} m_0. \quad (5.9)$$

Using eqs. (5.5), (5.6), we find that the overlap mass m_0 receives a multiplicative renormalization for massive HF, while for massless HF such renormalization is absent. For massless overlap fermions, the dependence on the coefficients in the HF kernel cancels completely in the limit of small momentum.

The resulting dispersion relations along three direction in the Brillouin zone are shown in figure 1 for overlap fermions with both a massless and a massive (with HF rest mass $m_R = 1$) HF kernel. Note that we fixed the overlap rest mass at 0.1 and determined the bare mass from eq. (5.9). It is clear that the improved scaling of the HF kernel ensures agreement with the continuum dispersion relation for much larger momenta. The deviation at larger momenta results in the behaviour $\partial E_{\mathbf{k}}/\partial \mathbf{k} > 1$, which is especially pronounced for the massless kernel.

The coefficients in the meson spectral functions are given in eq. (3.20), after multiplying $C_{\nu}(iE_{\mathbf{k}}, \mathbf{k})$ with $C_{\nu}^{\text{HF}}(iE_{\mathbf{k}}, \mathbf{k})$. The residue is given by eq. (A.9). Comparison of the coefficients and the residue with their continuum counterparts shows again that the fermion propagator receives a multiplicative renormalization. Expanding the HF overlap

propagator for small K and m_0 yields

$$S(K) \approx \frac{\mu^3(\mu - m_0/2)}{(\mu^2 + m_0^2/4)^2} \left[\frac{\mu - m_{\text{HF}}(0)}{\mu C_\nu^{\text{HF}}(0)} \frac{-iK + m_{\text{eff}}}{K^2 + m_{\text{eff}}^2} + \frac{1}{2\mu} \right], \quad (5.10)$$

where m_{eff} was defined above. For overlap fermions with a massive HF kernel we find therefore that both the overlap mass and the fermion propagator are renormalized by the factor $[\mu - m_{\text{HF}}(0)] / \mu C_\nu^{\text{HF}}(0)$.

Meson spectral functions with overlap hypercube fermions are shown in figure 5 for the pseudoscalar and figure 6 for the vector channel. Besides a factor of 2 (see table 1), these spectral functions differ in detail around the knee at $a\omega \sim 0.5$, which can be understood from the continuum expression (2.17). As expected, the first cusp in the spectral functions is shifted to substantially larger frequencies, determined by twice the maximal energy along the $(1, 0, 0)$ direction, yielding $a\omega \sim 3.75$ (5.0) for the massive (massless) HF kernel, as can be seen from figure 1 (top). As a result, the continuum behaviour at larger frequencies, $\rho(\omega) \sim \omega^2$, is better reproduced. However, we would like to point out that the contributions from these large frequencies are highly suppressed in the euclidean correlator. Taking for simplicity the zero temperature kernel $K(\tau, \omega) = e^{-\omega\tau} = e^{-a\omega n\tau}$, we find that already at the first time slice $K \sim e^{-5}$ when $a\omega \sim 5$, demonstrating the insensitivity to these large frequencies.

6. QCD with dynamical domain wall fermions

We now build on the free field calculations and consider spectral functions in QCD. Most spectral function studies to date have been carried out in quenched QCD; for recent work, see e.g. ref. [22] and references therein. A study of charmonium spectral functions in dynamical QCD with two flavours on highly anisotropic lattices can be found in ref. [23]. Spectral functions at nonzero momentum in quenched QCD are considered in refs. [24, 25].

In this section, we consider spectral functions at zero momentum, extracted from meson correlators obtained in dynamical lattice simulations. These correlators are computed using the domain wall fermion action on 2+1 flavour background configurations employing the Iwasaki gauge action [26, 27].⁶ This data has been generated by the RBC and UKQCD collaborations [29–33] on QCDOC [34–36]. Here, we present results obtained on a $16^3 \times 32$ lattice at $\beta = 2.13$ with an inverse lattice spacing of 1.6 GeV [33]. The number of points in the fifth dimension is $N_s = 16$.

In practical implementations of the domain wall fermion formalism it is important to choose a domain wall height that minimises the mixing between right and left-handed fermion modes at zero bare quark mass. This mixing, which vanishes in the limit $N_s \rightarrow \infty$, induces some residual chiral symmetry breaking and generates, for example, an additive quark mass renormalisation. In free field theory the optimal value for the domain wall height is unity. However, in the interacting theory, the domain wall height receives a large additive correction and the bare parameter should be adjusted accordingly [37, 38]. The

⁶Meson spectral functions using domain wall fermions in quenched QCD have been studied in ref. [28].

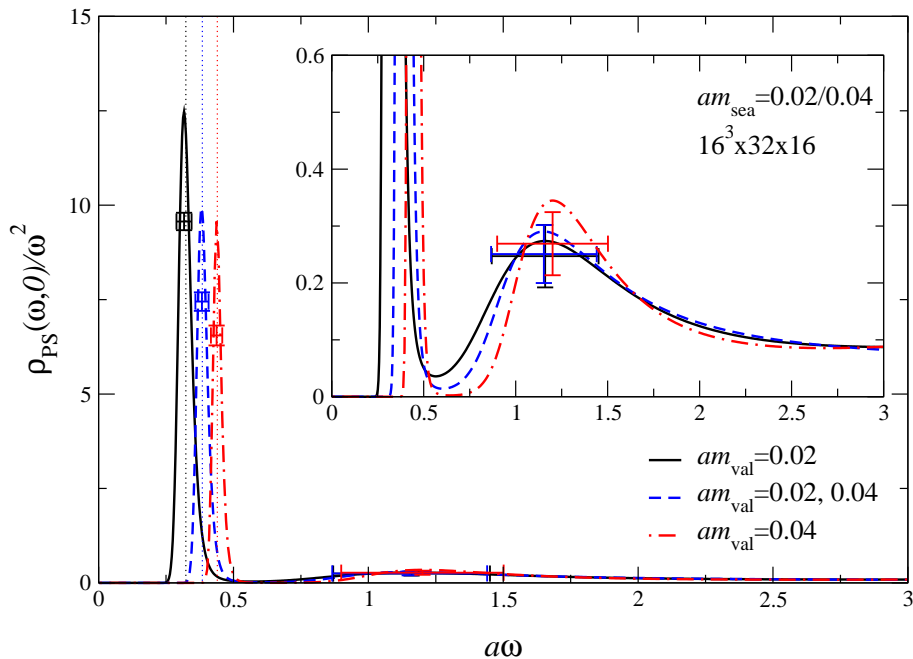


Figure 7: Pseudoscalar spectral functions in QCD with 2 + 1 flavours of dynamical domain wall fermions, determined using the Maximum Entropy Method, for different values of the valence quark masses. The vertical dotted lines indicate groundstate masses obtained with conventional cosh fits [29]. The inset shows a blow-up of the second bump.

bare domain wall height used in these simulations is $\mu = 1.8$. Subtracting a simple mean-field estimate for the radiative corrections [39] yields a value for the domain wall height of $\mu^{\text{MF}} = 1.3029$ [40], which is much closer to unity.

In this first study we show results obtained with a light bare sea quark mass $m_{ud} = 0.02$ and a heavier sea quark mass $m_s = 0.04$. To preserve unitarity, the valence quarks are constrained to take the same bare mass values as the sea quarks. To determine the spectral functions the Maximum Entropy Method [2] is applied to correlation functions measured on an ensemble of 70 independent gauge field configurations. The meson interpolating operators used are local quark field bilinears. The meson correlators are symmetric about the central time slice of the lattice. In our analysis we average the correlation functions over equivalent time slices and exclude the contact term at $\tau = 0$. The MEM algorithm uses Bryan’s method [41]. As the default model we take $\rho_{\text{default}}(\omega, \mathbf{0}) = m_0\omega^2$, where the constant m_0 is determined by a best fit to the data.

In figure 7 we show spectral functions obtained from pseudoscalar correlators evaluated for different valence quark masses. For each quark mass combination clear peaks are visible whose position corresponds to the energy of the lightest state that couples to the interpolating operators. The horizontal errorbars on these peaks give a measure of the peak width, while the vertical errorbars are inversely proportional to the significance of the peak. As expected, the position of the low-lying peak increases as the average valence quark mass is increased. The dotted vertical lines passing through each of these peaks indicate the values for the ground state energies obtained from double cosh fits to the correlators [29].

Therefore, for the groundstates we find that the results of the MEM analysis are in precise agreement with the results of conventional fitting techniques.

At higher frequencies, $1 < a\omega < 2$, second much broader bumps are visible. There appears to be no significant valence quark mass dependence of the position of these second peaks. We note that the heights of the bumps are of the same order as the structure due to the cusps observed in the free fermion calculation, for a domain wall height of unity.⁷ From our earlier analysis, we find therefore that the position of these bumps is not inconsistent with their identification as lattice artefacts. However, these peaks may also contain excited state contributions, but due to the width of the peaks these are difficult to resolve. An unambiguous way to disentangle excited state resonances from the contribution due to lattice artefacts is to carry out an analysis at different lattice spacings. With current data, this option is not yet available.⁸

7. Summary

We have analyzed meson spectral functions from lattice fermions with chiral symmetry. For free fermions, we have given a general prescription on how to construct lattice meson spectral functions from the euclidean fermion propagator, extending the analysis of ref. [4]. We have subsequently applied this to overlap fermions, domain wall fermions and overlap hypercube fermions. Lattice artefacts appear at (twice the) frequencies at which the lattice dispersion relation $E_{\mathbf{k}}$ deviates from the continuum relation. The most pronounced effect is the appearance of cusps at frequencies determined by $\partial E_{\mathbf{k}}/\partial \mathbf{k} = 0$. For most fermion formulations (Wilson, staggered, standard overlap, domain wall), these cusps appear at frequencies $1 < a\omega < 2$. In order to shift these artefacts to higher energies, it is necessary to use lattice fermions with improved scaling behaviour, such as hypercube fermions. In our spectral function analysis, we found that using the hypercube operator as a kernel in the overlap formalism indeed yields a formulation with good chiral and scaling behaviour, as could be anticipated from previous studies [11].

From a comparison between overlap and domain wall spectral functions, we found that the latter have a remarkably strong dependence on the domain wall height, whereas the dependence on the corresponding parameter in the case of the overlap operator is much milder. For a domain wall height of unity and a small fermion mass, we found that the overlap and domain wall spectral functions are comparable.

In the final section of the paper we have performed a Maximum Entropy analysis of pseudoscalar spectral functions in QCD with dynamical domain wall fermions, using data generated by the UKQCD and RBC collaborations. We found good agreement between the groundstate masses, determined by conventional cosh fits, and the position of the peak in the spectral functions. At larger frequencies, $1 < a\omega < 2$, a second peak can be seen.

⁷Note, however, that we have not applied wave function renormalization, which affects the vertical scale. Moreover, the free calculation indicates a strong dependence on the domain wall height, such that a quantitative comparison would require knowledge of the renormalized domain wall height.

⁸Unphysical structure at higher frequencies has also been observed in quenched simulations with Wilson fermions. In refs. [42, 43] this was interpreted as bound states of Wilson doublers.

We have argued that this structure is not inconsistent with the lattice artefacts found in the analytical study, although the presence of excited states cannot be excluded. An unambiguous way to distinguish (physical) excited states from (unphysical) lattice artefacts discussed here, is to repeat the analysis at different lattice spacings.

Acknowledgments

We thank Chris Allton and Jonathan Clowser for providing us with a Maximum Entropy routine and easy access to the dynamical domain wall correlation functions. We thank Dave Antonio, Peter Boyle, Brian Pendleton and Rob Tweedie for the generation of the non-perturbative DWF data, which is part of the UKQCD and RBC collaborations joint research programme. We also thank our colleagues in the UKQCD and RBC collaborations. The data was obtained using the QCDOC computers installed at the University of Edinburgh and Brookhaven National laboratory. We thank PPARC (JIF grant PPA/J/S/1998/00756), RIKEN, Brookhaven National Laboratory and the U.S. Department of Energy for these facilities. G.A. is supported by a PPARC Advanced Fellowship.

A. More on overlap hypercube fermions

In this appendix we collect some expressions for overlap hypercube fermions, discussed in section 5.

The pole is determined by

$$\sum_{\nu} C_{\nu}^{\text{HF}^2}(K) \sin^2 k_{\nu} = -\bar{m}_0^2 b^2(K), \quad b(K) < 0, \quad (\text{A.1})$$

where \bar{m}_0 was defined in eq. (3.7). In order to solve for the dispersion relation, we follow ref. [3] and use the notation

$$\begin{aligned} C_4^{\text{HF}}(K) &= \delta_{\mathbf{k}}, \\ C_i^{\text{HF}}(K) \sin k_i &= \alpha_{i\mathbf{k}} + \beta_{i\mathbf{k}} \cos k_4, \\ m_{\text{HF}}(K) &= \kappa_{1\mathbf{k}} + \kappa_{2\mathbf{k}} \cos k_4, \end{aligned} \quad (\text{A.2})$$

and

$$\alpha_{\mathbf{k}}^2 = \sum_{i=1}^3 \alpha_{i\mathbf{k}}^2, \quad \beta_{\mathbf{k}}^2 = \sum_{i=1}^3 \beta_{i\mathbf{k}}^2, \quad \alpha_{\mathbf{k}} \cdot \beta_{\mathbf{k}} = \sum_{i=1}^3 \alpha_{i\mathbf{k}} \beta_{i\mathbf{k}}. \quad (\text{A.3})$$

Expressions for $\alpha_{i\mathbf{k}}$, $\beta_{i\mathbf{k}}$, $\delta_{\mathbf{k}}$, and $\kappa_{1,2\mathbf{k}}$ can easily be derived from these definitions combined with eqs. (5.3), (5.4). Explicit expressions are given in eqs. (B.1-B.9) of ref. [3].

Writing $k_4 = iE_{\mathbf{k}}$ yields again a quadratic equation for $\cosh E_{\mathbf{k}}$, where the allowed solution is of the form

$$\cosh E_{\mathbf{k}} = \frac{x_{\mathbf{k}} + \sqrt{y_{\mathbf{k}}}}{z_{\mathbf{k}}}, \quad (\text{A.4})$$

with

$$\begin{aligned}
 x_{\mathbf{k}} &= \alpha_{\mathbf{k}} \cdot \beta_{\mathbf{k}} + \bar{m}_0^2 \kappa_{2\mathbf{k}} (\kappa_{1\mathbf{k}} - \mu), \\
 y_{\mathbf{k}} &= (\alpha_{\mathbf{k}} \cdot \beta_{\mathbf{k}})^2 + (\delta_{\mathbf{k}}^2 - \beta_{\mathbf{k}}^2) (\delta_{\mathbf{k}}^2 + \alpha_{\mathbf{k}}^2) \\
 &\quad + \bar{m}_0^2 \left[2 (\alpha_{\mathbf{k}} \cdot \beta_{\mathbf{k}}) \kappa_{2\mathbf{k}} (\kappa_{1\mathbf{k}} - \mu) + (\kappa_{1\mathbf{k}} - \mu)^2 (\delta_{\mathbf{k}}^2 - \beta_{\mathbf{k}}^2) - \kappa_{2\mathbf{k}}^2 (\delta_{\mathbf{k}}^2 + \alpha_{\mathbf{k}}^2) \right], \\
 z_{\mathbf{k}} &= \delta_{\mathbf{k}}^2 - \beta_{\mathbf{k}}^2 - \bar{m}_0^2 \kappa_{2\mathbf{k}}^2.
 \end{aligned} \tag{A.5}$$

The root $(x_{\mathbf{k}} - \sqrt{y_{\mathbf{k}}})/z_{\mathbf{k}} < 0$ for all momenta inside the Brillouin zone and therefore not a valid solution, in contrast to the standard HF case.

The rest mass is given by

$$\cosh E_0 = \frac{\bar{m}_0^2 \kappa_{20} (\kappa_{10} - \mu) + \delta_0 \sqrt{\delta_0^2 + \bar{m}_0^2 [(\kappa_{10} - \mu)^2 - \kappa_{20}^2]}}{\delta_0^2 - \bar{m}_0^2 \kappa_{20}^2}, \tag{A.6}$$

where

$$\kappa_{10} = \lambda^{(0)} + 6\lambda^{(1)} + 12\lambda^{(2)} + 8\lambda^{(3)}, \tag{A.7}$$

$$\kappa_{20} = 2\lambda^{(1)} + 12\lambda^{(2)} + 24\lambda^{(3)} + 16\lambda^{(4)}. \tag{A.8}$$

The explicit expression for the residue reads

$$\frac{1}{\mathcal{E}_{\mathbf{k}}} = \frac{\mu}{\mu^2 + \bar{m}_0^2/4 (\delta_{\mathbf{k}}^2 - \beta_{\mathbf{k}}^2) \cosh E_{\mathbf{k}} - \alpha_{\mathbf{k}} \cdot \beta_{\mathbf{k}} - \bar{m}_0^2 \kappa_{2\mathbf{k}} b(iE_{\mathbf{k}}, \mathbf{k})} \frac{1}{\sinh E_{\mathbf{k}}} \frac{\omega(iE_{\mathbf{k}}, \mathbf{k})}{\sinh E_{\mathbf{k}}}. \tag{A.9}$$

There exists no pole at $k_4 = \pi - iE_{\mathbf{k}}$, provided $b(K) = m_{\text{HF}}(K) - \mu > 0$, or

$$\mu < \kappa_{1\mathbf{k}} - \kappa_{2\mathbf{k}} \cosh E_{\mathbf{k}}. \tag{A.10}$$

Since $\kappa_{1,2\mathbf{k}}$ depend on in a nontrivial manner on the coefficients in the HF kernel, this constraint on μ has to be verified on a case by case situation.

References

- [1] M. Jarrell and J.E. Gubernatis, *Bayesian inference and the analytic continuation of imaginary-time quantum Monte Carlo data*, *Phys. Rept.* **269** (1996) 133.
- [2] M. Asakawa, T. Hatsuda and Y. Nakahara, *Maximum entropy analysis of the spectral functions in lattice QCD*, *Prog. Part. Nucl. Phys.* **46** (2001) 459 [[hep-lat/0011040](#)].
- [3] F. Karsch, E. Laermann, P. Petreczky and S. Stickan, *Infinite temperature limit of meson spectral functions calculated on the lattice*, *Phys. Rev.* **D 68** (2003) 014504 [[hep-lat/0303017](#)].
- [4] G. Aarts and J.M. Martínez Resco, *Continuum and lattice meson spectral functions at nonzero momentum and high temperature*, *Nucl. Phys.* **B 726** (2005) 93 [[hep-lat/0507004](#)].
- [5] R. Narayanan and H. Neuberger, *Infinitely many regulator fields for chiral fermions*, *Phys. Lett.* **B 302** (1993) 62 [[hep-lat/9212019](#)]; *A construction of lattice chiral gauge theories*, *Nucl. Phys.* **B 443** (1995) 305 [[hep-th/9411108](#)].

- [6] H. Neuberger, *Exactly massless quarks on the lattice*, *Phys. Lett. B* **417** (1998) 141 [[hep-lat/9707022](#)]; *More about exactly massless quarks on the lattice*, *Phys. Lett. B* **427** (1998) 353 [[hep-lat/9801031](#)].
- [7] D.B. Kaplan, *A method for simulating chiral fermions on the lattice*, *Phys. Lett. B* **288** (1992) 342 [[hep-lat/9206013](#)].
- [8] Y. Shamir, *Chiral fermions from lattice boundaries*, *Nucl. Phys. B* **406** (1993) 90 [[hep-lat/9303005](#)].
- [9] V. Furman and Y. Shamir, *Axial symmetries in lattice QCD with Kaplan fermions*, *Nucl. Phys. B* **439** (1995) 54 [[hep-lat/9405004](#)].
- [10] W. Bietenholz, *Solutions of the Ginsparg-Wilson relation and improved domain wall fermions*, *Eur. Phys. J. C* **6** (1999) 537 [[hep-lat/9803023](#)].
- [11] W. Bietenholz and I. Hip, *The scaling of exact and approximate Ginsparg-Wilson fermions*, *Nucl. Phys. B* **570** (2000) 423 [[hep-lat/9902019](#)].
- [12] S. Wissel, E. Laermann, S. Shcheredin, S. Datta and F. Karsch, *Meson correlation functions at high temperatures*, *PoS(LAT2005)164* [[hep-lat/0510031](#)].
- [13] W. Bietenholz and S. Shcheredin, *Overlap hypercube fermions in QCD*, *Nucl. Phys.* **153** (*Proc. Suppl.*) (2006) 17 [[hep-lat/0511051](#)].
- [14] D.B. Carpenter and C.F. Baillie, *Free fermion propagators and lattice finite size effects*, *Nucl. Phys. B* **260** (1985) 103.
- [15] G. Aarts and J.M. Martinez Resco, *Transport coefficients, spectral functions and the lattice*, *JHEP* **04** (2002) 053 [[hep-ph/0203177](#)]; *Transport coefficients from the lattice?*, *Nucl. Phys.* **119** (*Proc. Suppl.*) (2003) 505 [[hep-lat/0209033](#)].
- [16] S. Capitani, *Lattice perturbation theory*, *Phys. Rept.* **382** (2003) 113 [[hep-lat/0211036](#)].
- [17] P. Hasenfratz and F. Niedermayer, *Perfect lattice action for asymptotically free theories*, *Nucl. Phys. B* **414** (1994) 785 [[hep-lat/9308004](#)].
- [18] P. Hasenfratz, *The theoretical background and properties of perfect actions*, [hep-lat/9803027](#).
- [19] W. Bietenholz, R. Brower, S. Chandrasekharan and U.J. Wiese, *Progress on perfect lattice actions for QCD*, *Nucl. Phys.* **53** (*Proc. Suppl.*) (1997) 921 [[hep-lat/9608068](#)].
- [20] W. Bietenholz and U.J. Wiese, *Perfect lattice actions for quarks and gluons*, *Nucl. Phys. B* **464** (1996) 319 [[hep-lat/9510026](#)].
- [21] W. Bietenholz, *Optimised dirac operators on the lattice: construction, properties and applications*, [hep-lat/0611030](#).
- [22] A. Jakovac, P. Petreczky, K. Petrov and A. Velytsky, *Quarkonium correlators and spectral functions at zero and finite temperature*, *Phys. Rev. D* **75** (2007) 014506 [[hep-lat/0611017](#)].
- [23] G. Aarts et al., *Charmonium spectral functions in $N(f) = 2$ QCD at high temperature*, *PoS(LAT2006)126* [[hep-lat/0610065](#)]; *Charmonium spectral functions in two-flavour QCD*, [hep-lat/0608009](#);
R. Morrin et al., *Charmonium spectral functions in $N(f) = 2$ QCD*, *PoS(LAT2005)176* [[hep-lat/0509115](#)].
- [24] S. Datta, F. Karsch, S. Wissel, P. Petreczky and I. Wetzorke, *Charmonia at finite momenta in a deconfined plasma*, [hep-lat/0409147](#).

- [25] G. Aarts, C. Allton, J. Foley, S. Hands and S. Kim, *Spectral functions at non-zero momentum in hot QCD*, hep-lat/0610061; *Meson spectral functions at nonzero momentum in hot QCD*, hep-lat/0607012.
- [26] Y. Iwasaki and T. Yoshie, *Renormalization group improved action for SU(3) lattice gauge theory and the string tension*, *Phys. Lett. B* **143** (1984) 449.
- [27] Y. Iwasaki, *Renormalization group analysis of lattice theories and improved lattice action: two-dimensional nonlinear $O(N)$ sigma model*, *Nucl. Phys. B* **258** (1985) 141.
- [28] T. Blum and P. Petreczky, *Cutoff effects in meson spectral functions*, *Nucl. Phys.* **140** (Proc. Suppl.) (2005) 553 [hep-lat/0408045].
- [29] UKQCD and RBC collaboration, C. Allton et al., *Light meson masses and non-perturbative renormalisation in 2 + 1 flavour domain wall QCD*, hep-lat/0610119.
- [30] UKQCD and RBC collaboration, D.J. Antonio et al., *Production and properties of 2 + 1 flavour DWF ensembles*, PoS(LAT2006)188.
- [31] Min Li, *The static quark potential for dynamical domain wall fermions*, PoS(LAT2006)183.
- [32] D.J. Antonio et al., *First results from 2 + 1-flavor domain wall QCD: mass spectrum, topology change and chiral symmetry with $L_s = 8$* , hep-lat/0612005.
- [33] C. Allton et al., *2 + 1 flavor domain wall QCD on a $(2\text{ fm})^3$ lattice: light meson spectroscopy with $L_s = 16$* , hep-lat/0701013.
- [34] P. Boyle et al., *The QCDOC project*, *Nucl. Phys.* **140** (Proc. Suppl.) (2005) 169.
- [35] P.A. Boyle et al., *Hardware and software status of QCDOC*, *Nucl. Phys.* **129** (Proc. Suppl.) (2004) 838 [hep-lat/0309096].
- [36] QCDOC collaboration, P.A. Boyle, C. Jung and T. Wettig, *The qcdoc supercomputer: hardware, software and performance*, *ECONF C0303241* (2003) THIT003 [hep-lat/0306023].
- [37] T. Blum and A. Soni, *QCD with domain wall quarks*, *Phys. Rev. D* **56** (1997) 174 [hep-lat/9611030].
- [38] T. Blum, A. Soni and M. Wingate, *Calculation of the strange quark mass using domain wall fermions*, *Phys. Rev. D* **60** (1999) 114507 [hep-lat/9902016].
- [39] S. Aoki, T. Izubuchi, Y. Kuramashi and Y. Taniguchi, *Perturbative renormalization factors in domain-wall QCD with improved gauge actions*, *Phys. Rev. D* **67** (2003) 094502 [hep-lat/0206013].
- [40] UKQCD collaboration, P.A. Boyle et al., *A lattice computation of the first moment of the kaon's distribution amplitude*, *Phys. Lett. B* **641** (2006) 67 [hep-lat/0607018].
- [41] R.K. Bryan, *Maximum entropy analysis of oversampled data problems* *Eur. Biophys. J.* **18** (1990) 165.
- [42] CP-PACS collaboration, T. Yamazaki et al., *Spectral function and excited states in lattice QCD with maximum entropy method*, *Phys. Rev. D* **65** (2002) 014501 [hep-lat/0105030].
- [43] K. Sasaki, S. Sasaki and T. Hatsuda, *Spectral analysis of excited nucleons in lattice QCD with maximum entropy method*, *Phys. Lett. B* **623** (2005) 208 [hep-lat/0504020].